ARTICLES
https://doi.org/10.1038/s41559-019-0914-2
nature ecology & evolution

Historical contingency shapes adaptive radiation in Antarctic fishes

Jacob M. Daane[1*], Alex Dornburg[2], Patrick Smits[3], Daniel J. MacGuigan[4], M. Brent Hawkins[3,5,6], Thomas J. Near[4,7], H. William Detrich III[1,8*] and Matthew P. Harris[3,6,8*]

Adaptive radiation illustrates links between ecological opportunity, natural selection and the generation of biodiversity. Central to adaptive radiation is the association between a diversifying lineage and the evolution of phenotypic variation that facilitates the use of new environments or resources. However, is not clear whether adaptive evolution or historical contingency is more important for the origin of key phenotypic traits in adaptive radiation. Here we use targeted sequencing of >250,000 loci across 46 species to examine hypotheses concerning the origin and diversification of key traits in the adaptive radiation of Antarctic notothenioid fishes. Contrary to expectations of adaptive evolution, we show that notothenioids experienced a punctuated burst of genomic diversification and evolved key skeletal modifications before the onset of polar conditions in the Southern Ocean. We show that diversifying selection in pathways associated with human skeletal dysplasias facilitates ecologically important variation in buoyancy among Antarctic notothenioid species, and demonstrate the sufficiency of altered *trip11*, *col1a2* and *col1a1a* function in zebrafish (*Danio rerio*) to phenocopy skeletal reduction in Antarctic notothenioids. Rather than adaptation being driven by the cooling of the Antarctic, our results highlight the role of historical contingency in shaping the adaptive radiation of notothenioids. Understanding the historical and environmental context for the origin of key traits in adaptive radiations extends beyond reconstructing events that result in evolutionary innovation, as it also provides a context in forecasting the effects of climate change on the stability and evolvability of natural populations.

During adaptive radiation, ecological opportunity and key phenotypic traits interact to facilitate the expansion of populations into new niches[1]. Deciphering the genotype–phenotype relationships of these key traits provides important insight into the historical circumstances that result in phenotypic diversification[2,3]. Advances in sequencing capabilities now allow for the efficient collection of genomic sequence data for scores of species. This potential for increased taxonomic, genome-wide sampling provides opportunities to investigate the macro-evolutionary mechanisms driving evolution across clades. For example, a major question in the study of adaptive radiation is the relative role of trait novelty versus the modification of existing phenotypes in facilitating the diversification of species. Ecological opportunities, such as those brought about by environmental changes, can promote the origin of novel phenotypes that accelerate lineage diversification[4–7]. However, trait novelty may arise at any time and adaptive change can result from a shift in selection regimes that enable lineages to opportunistically explore new ecospace using a trait that had previously evolved under different circumstances[8]. These two hypotheses have long been central to the debate concerning the role of punctuated versus gradualistic evolution in the generation of biodiversity[8,9], and posit opposing views on how the genomic substrate of subsequent phenotypic diversification evolved. Here, we provide a genomic perspective of ecologically important trait variation and phylogenetic origin in a species-rich adaptive radiation. Through consideration of closely related lineages that are not a part of the adaptive radiation, we can specifically investigate the relative importance of contingency in adaptive radiation and test whether the genomic basis of ecological trait variation coincides with or precedes the onset of radiation.

Results and discussion

To test hypotheses concerning the origin of traits that facilitate adaptive radiation, we focused on Antarctic notothenioids (Cryonotothenioidea), an iconic example of adaptive radiation in marine vertebrates[10,11]. The diversification of cryonotothenioids followed the progressive cooling of Antarctica that initiated ~33 million years ago[10], and was coincident with the extinction of a phylogenetically diverse and cosmopolitan fish fauna[12]. This combination of climate change and vacated niches presented notothenioids with the opportunity to diversify into a large range of benthic and water column habitats. All notothenioids lack a swim bladder, the primary buoyancy organ in most teleost fishes; however, there are substantial differences in buoyancy among notothenioid species that are correlated with habitat and resource use[10,12]. These differences in buoyancy are achieved through the reduction of skeletal density coupled with the accumulation of corporeal lipids that provide static lift[12–14]. In the narrative of the Antarctic cryonotothenioid adaptive radiation, these ecologically important traits are hypothesized to have arisen during the onset of polar conditions; however, the evolutionary origin of reduced skeletal density in the context of early-diverging non-Antarctic notothenioid lineages challenges this scenario[14].

To develop a comprehensive phylogenomic perspective on the Antarctic notothenioid adaptive radiation, we employed a

[1]Department of Marine and Environmental Sciences, Northeastern University Marine Science Center, Nahant, MA, USA. [2]North Carolina Museum of Natural Sciences, Raleigh, NC, USA. [3]Orthopaedic Research Laboratories, Department of Orthopaedic Surgery, Boston Children's Hospital, Boston, MA, USA. [4]Department of Ecology and Evolutionary Biology, Yale University, New Haven, CT, USA. [5]Museum of Comparative Zoology, Harvard University, Cambridge, MA, USA. [6]Department of Genetics, Harvard Medical School, Boston, MA, USA. [7]Peabody Museum of Natural History, Yale University, New Haven, CT, USA. [8]These authors contributed equally: H. William Detrich III, Matthew P. Harris. *e-mail: j.daane@northeastern.edu; w.detrich@northeastern.edu; harris@genetics.med.harvard.edu

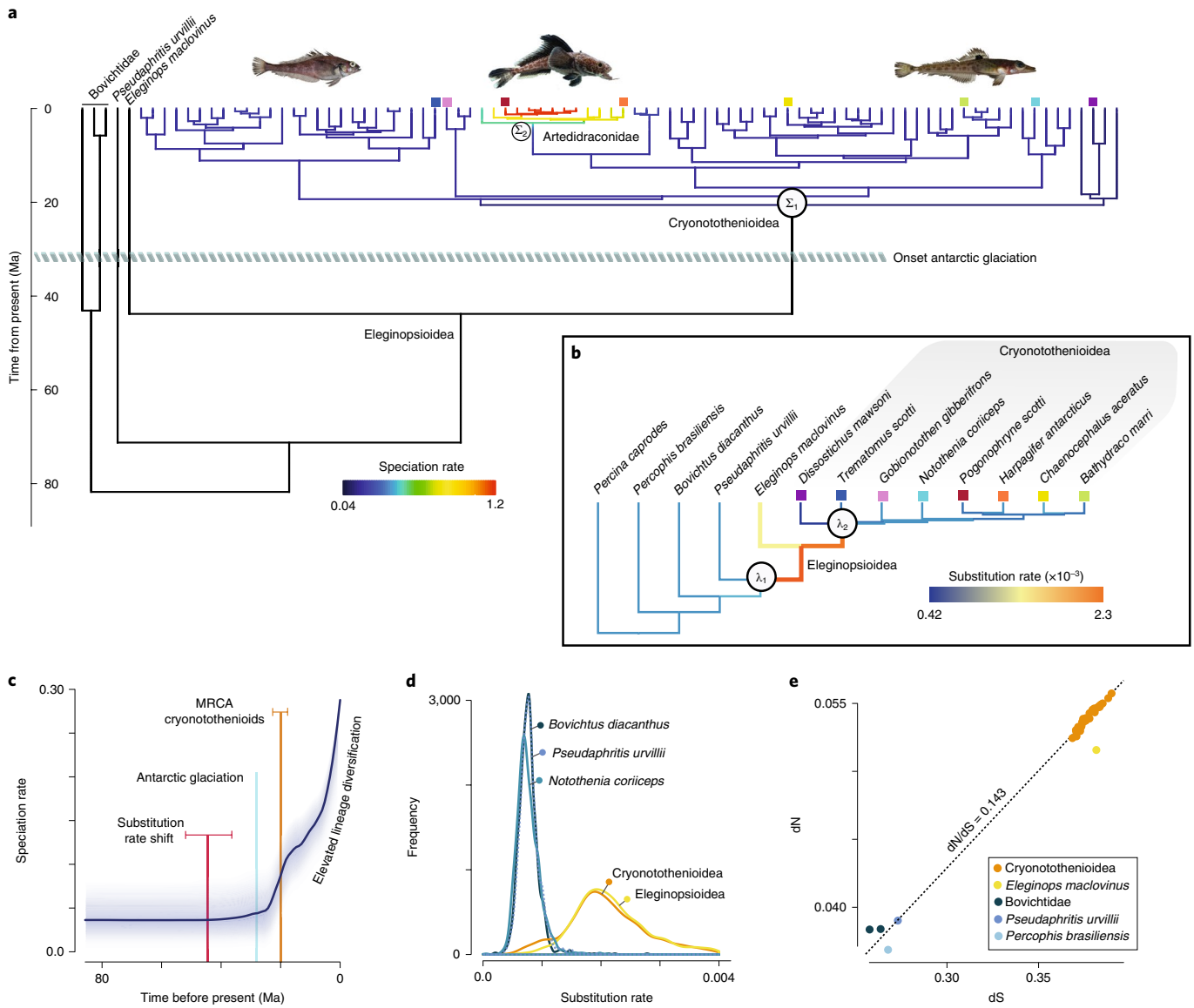

Fig. 1 | Punctuated elevation in genomic diversification before ecological change and adaptive radiation. a, Bayesian analysis of lineage diversification rates on the time-calibrated notothenioid phylogeny[11,18]. Σ indicates change in speciation rate; colours on branches correspond to the mean of the marginal posterior density of estimated speciation rates, with a shift from low (mean = 0.046 lineages Ma^{-1}) to faster rates of speciation (mean = 0.179 lineages Ma^{-1}) at the onset of the notothenioid adaptive radiation. Coloured squares at selected tips in phylogeny refer to corresponding species in **b**. **b**, Relaxed molecular clock model of nucleotide substitution rates (substitutions $site^{-1}$ Ma^{-1}) during notothenioid evolution, revealing a transient elevation in substitution rate before the increase in species diversification. Substitution rates were estimated from 1,062 independent gene trees constructed using the random local clock model in BEAST2. λ_1 indicates change in substitution rate, from an ancestral baseline of 7.7×10^{-4} substitutions $site^{-1}$ Ma^{-1} (95% highest posterior density (HPD) interval, 5.0×10^{-4}, 1.1×10^{-3}) to 2.3×10^{-3} substitutions $site^{-1}$ Ma^{-1} (95% HPD, 1.0×10^{-3}, 3.9×10^{-3}) observed on the branch leading to *E. maclovinus* and all cryonotothenioids. λ_2 indicates return to baseline substitution rate in cryonotothens, ranging from 4.2×10^{-4} substitutions $site^{-1}$ Ma^{-1} in *Dissostichus mawsoni* (95% HPD, 1.0×10^{-4}, 9.0×10^{-4}) to 7.7×10^{-4} substitutions $site^{-1}$ Ma^{-1} in *Chaenocephalus aceratus* (95% HPD, 2.0×10^{-4}, 2.2×10^{-3}). See Supplementary Table 4 for additional rates and 95% HPD. Colours on branches correspond to mean substitution rate. **c**, Elevation in speciation rate well after increase in nucleotide substitution rate and climate change events that precipitated adaptive diversification. Shading indicates 10–90% Bayesian credible region across time. Error bars for age of cryonotothenioid MRCA and time of substitution rate shift at MRCA of *Eleginops* and cryonotothenioids based on 95% Bayesian credible interval. **d**, Distribution of substitution rates from select species in **b**. **e**, Average dS and dN substitution rates from over 4,000 pairwise alignments for each species relative to the outgroup, *P. caprodes*. This shows an increase in overall substitution rate (dN and dS) without a genome-wide change in diversifying selection (dN/dS).

cross-species targeted sequence enrichment approach to specifically sequence conserved and functionally annotated genetic loci[15]. We combined sequence information from the genome of *Notothenia coriiceps* and other percomorph species to design a comparative DNA probe set for systematic targeted enrichment of ~250,000 coding and conserved non-coding elements (CNEs) comprising over 40 Mb of genomic sequence (Supplementary Fig. 1). CNEs were defined as microRNA (miRNA) hairpins, orthologues to human ultraconservative elements and constrained genetic regions identified in the Ensembl compara 11-way teleost genome alignment that did not overlap with protein-coding regions. Using this probe set, we captured coding and non-coding sequences from a

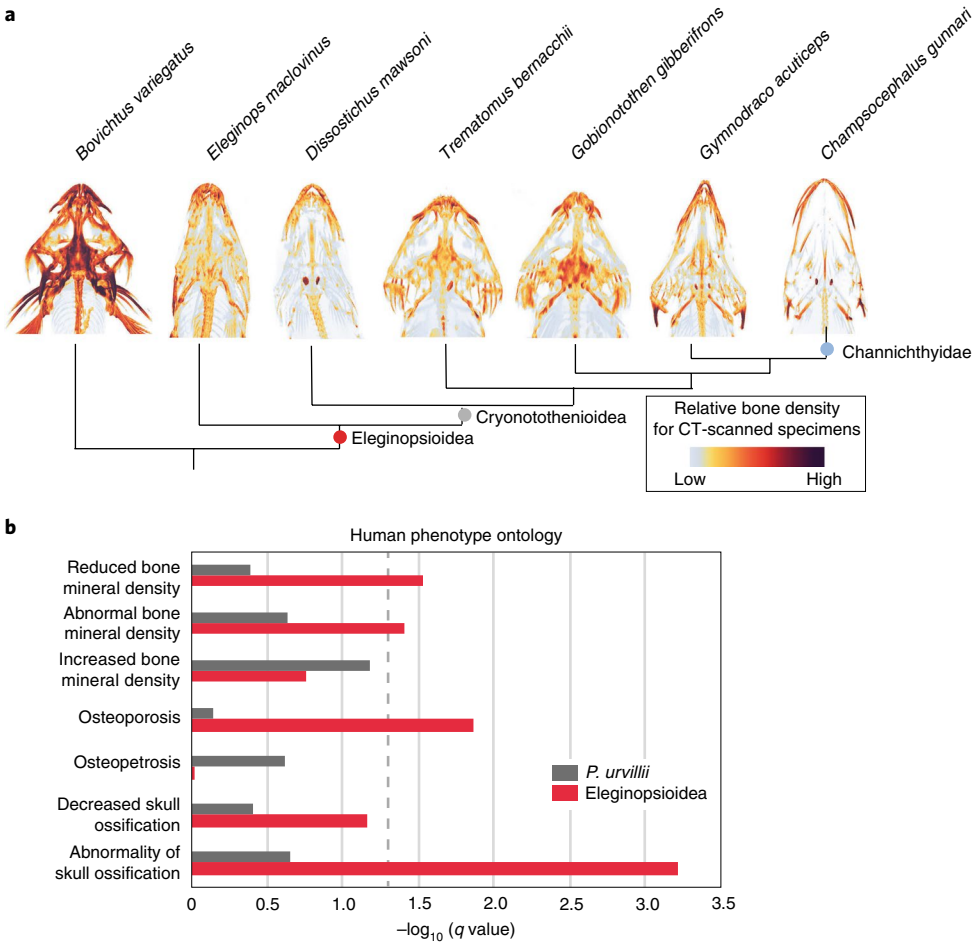

Fig. 2 | Skeletal reduction occurs before the cryonotothenioid radiation. a, Computed tomography of notothenioid skulls showing relative skeletal density across the phylogeny and decrease in skeletal density before cryonotothenioid radiation. CT, computed tomography. **b**, Comparison of significance of enrichment for polygenic selection on representative bone density-associated HPO terms between Eleginopsioidea and well-ossified sister group *P. urvillii*. Dashed line indicates false discovery rate $q < 0.05$ for SUMSTAT gene set enrichment test.

phylogenetically rich sampling of 46 notothenioid species that includes all three early-diverging non-Antarctic lineages and two species from the closely related Percidae (Supplementary Fig. 1). Importantly, we used pooled-population samples of individual species to permit identification of fixed and variable single-nucleotide polymorphisms (SNPs) for each species.

We achieved 88–95% coverage of targeted regions for each sampled species (Supplementary Fig. 1 and Supplementary Tables 1 and 2). This permitted identification of an average of 95,000 fixed species-specific SNPs and 60,000 heterozygous SNPs for each lineage (Supplementary Table 3). As proof of the sensitivity of the dataset, we confirmed known cases of adult haemoglobin gene loss within the icefishes (Supplementary Fig. 2)[16]. The power of this dataset was further illustrated by identification of a previously uncharacterized deletion of two putative embryonic haemoglobin genes (Supplementary Fig. 2). Thus, this approach provides a robust and efficient method by which to characterize variation across taxonomically rich clades, even when separated by major evolutionary distances.

Given expectations from the adaptive radiation of East African cichlids[17], we tested whether shifts in the rate of nucleotide evolution would correspond to the onset of rapid lineage diversification in the cryonotothenioid radiation. Using a time-calibrated phylogeny of most living notothenioids and a Bayesian framework to assess shifts in speciation rates[11,18], we confirmed a shift in lineage diversification at the origin of the antifreeze-bearing Antarctic cryonotothenioids and an additional acceleration in diversification within the Plunderfishes (Artedidraconidae)[10] (Fig. 1a). Intriguingly, these shifts do not correspond to accelerated rates of nucleotide evolution. Instead, we found that the majority of extant cryonotothenioid sequence diversity is derived from a period of very high rates of genomic evolution that occurred in the ancestral lineage that includes the most recent common ancestor of the non-Antarctic distributed *Eleginops maclovinus* and the Antarctic cryonotothenioids (Eleginopsioidea; Fig. 1b and Supplementary Table 4). This demonstrates that a major change in molecular rate variation preceded the onset of global cooling and adaptive radiation of cryonotothenioids by well over ten million years (Fig. 1c). An assessment of the accumulation of genomic divergence through relaxed molecular clock models (Fig. 1d), along with an analysis of synonymous (dS) and non-synonymous substitution (dN) rates (Fig. 1e), further substantiates a high rate of nucleotide evolution before the origin and diversification of cryonotothenioids. This acceleration of overall genomic change may have been critical for accumulation of the genetic diversity that provided the substrate for phenotypic diversification during the early radiation of cryonotothenioids.

As buoyancy adaptations are key traits that facilitated notothenioid diversification into the water column during the adaptive radiation, we assessed patterns of skeletal density throughout the phylogeny using computerized tomography (Fig. 2a and

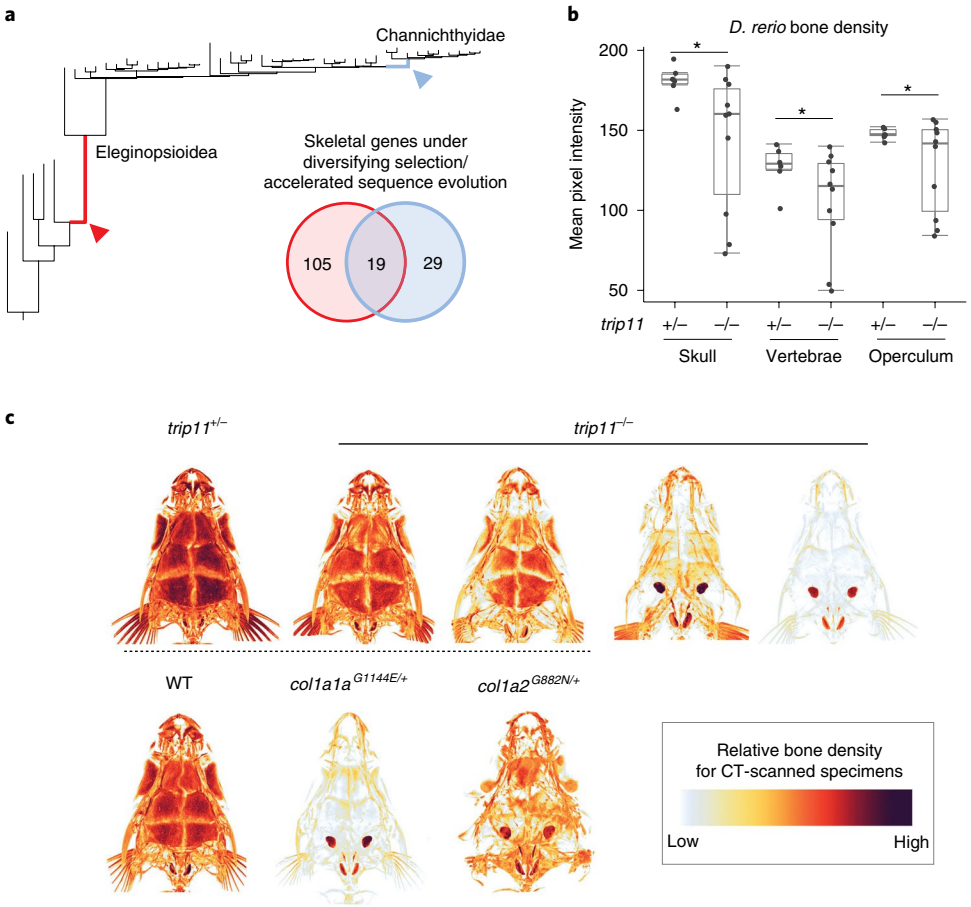

Fig. 3 | Skeletal genes under diversifying selection uncover genetic mechanisms regulating bone density. a, Comparison of genes under positive selection (aBSREL, $P < 0.05$) and/or accelerated sequence evolution (phyloP, $P < 0.05$) on the branch leading to *E. maclovinus* and Antarctic cryonotothenioids (Eleginopsioidea) with the branch leading to the icefishes, Channichthyidae. **b**, Quantitation of skeletal density from micro-computed tomography (μCT) analysis of zebrafish mutants in *trip11*. Density is the average pixel intensity; $n = 6$ scanned *trip11*$^{+/-}$ and $n = 10$ *trip11*$^{-/-}$ individuals. Centre line is mean density, box bounds indicate lower and upper quartiles, whiskers extend to a maximum of 1.5× the interquartile range. *, one-tailed *t*-test $P < 0.05$. **c**, μCT of zebrafish showing reduction in bone density in the cranium of zebrafish mutant models of genes under selection in Eleginopsioidea. Representative μCT images of zebrafish skulls from heterozygous and homozygous *trip11* mutants, showing reduced bone density and variable penetrance. Reduction in density in the cranium caused by mutations in *col1a1a*$^{dmh14/+}$ (G1144E) and *col1a2*$^{dmh15/+}$ (G882N).

Supplementary Fig. 3). We find that, in parallel with the observed increase in nucleotide substitution rate, a broad reduction in bone density occurred before the recent common ancestor of *E. maclovinus*[14] and the Antarctic cryonotothenioids (Eleginopsioidea, Fig. 2a) and was retained throughout the clade. Consistent with these decreases in bone density, we found biased diversifying selection in genes associated with human skeletal dysplasias and mineralization defects in Eleginopsioidea relative to the well-ossified sister lineage, *Pseudaphritis urvillii* (Fig. 2b,c). This evolutionary reconstruction is contrary to the expectation of the emergence of novel traits temporally coinciding with the onset of adaptive radiation and changing ecological opportunities. Instead, our results indicate that, before the shift to polar conditions, notothenioid lineages possessed key traits and may have begun to use new habitats in the water column through a modification of buoyancy enabled through a derived reduction in bone density.

To further explore the genetic basis of the evolved reduction in bone density, we assessed patterns of diversifying selection within the phylogeny. Among *E. maclovinus* and all cryonotothenioids, we identified shared selective signatures in clinically relevant skeletal genes, such as *collagen1a1a* and *collagen1a2* (Fig. 3a, Supplementary Figs. 4–6 and Supplementary Table 5). The function of these genes is conserved among disparate lineages of vertebrates[19], and non-synonymous mutations in these collagens can lead to severe osteogenesis imperfecta in humans[20]. Notably, previous studies show that *collagen1* expression is reduced in the developing skeleton of notothenioid embryos, providing further evidence that broad changes at *collagen* loci are associated with skeletal variation[21]. In addition to selection on collagens, we identified diversifying selection in an unlikely gene candidate for skeletal variation, *trip11*(*gmap-210*) (Fig. 3a, Supplementary Figs. 4–6 and Supplementary Table 5). This gene is conserved across eukaryotes and functions in vesicle tethering in the cis-Golgi membrane[22]. In humans, mutations in *TRIP11* lead to severe skeletal deficiencies that then result in perinatal lethality[23]. Intriguingly, both *collagen1a1a* and *trip11* are also under diversifying selection and/or accelerated sequence evolution within the further diversification of the Channichthyidae, which have evolved an additional and major reduction in bone density (Figs. 2a and 3a, Supplementary Figs. 4–6 and Supplementary Tables 5–8)[14]. This parallelism suggests constraint in the types of mutations in evolution that can drive changes in skeletal density while maintaining viability.

To experimentally test the potential for alterations in *trip11*, *col1a1a* and *col1a2* function to impart non-lethal skeletal phenotypes that are consistent with those observed in notothenioids, we analysed mutants stemming from genetic screens and

CRISPR-Cas9 gene editing in *D. rerio*. Contrary to expectations from humans, zebrafish homozygous for loss-of-function alleles of *trip11* were viable with no obvious external morphological abnormalities (Fig. 3b,c). However, whereas heterozygous siblings had density patterns comparable to wild-type (WT) zebrafish, similarly sized and age-matched homozygous *trip11* mutants had significantly reduced skeletal density (Fig. 3b,c). In affected individuals, all bones investigated, including those of the skull roof, vertebrae and operculum, were reduced in density (Fig. 3b,c) and generally phenocopied the pattern observed in adult *E. maclovinus* and cryonotothenioids (Fig. 2a). Notably, expressivity of the *trip11* skeletal phenotype was variable, which suggests the presence of background genetic modifiers. Similarly, we show that mutant models of *col1a1a*$^{dmh14/+}$ (G1144E) and *col1a2*$^{dmh15/+}$ (G882N) in zebrafish also cause a reduction in bone density (Fig. 3c)[19]. These experiments confirm that changes to the loci under selection yield phenotypes consistent with those observed in *E. maclovinus* and species of the cryonotothenioid radiation.

Our results reveal that historical contingency was a major factor in shaping the adaptive radiation of notothenioids. Because the onset of polar conditions ~33 Ma (million years ago) decimated the teleost fauna of the Southern Ocean, notothenioids were the only surviving lineage poised to occupy newly open niche space in a range of benthic and water column habitats[24]. Rather than being driven by directional selection to evolve extreme phenotypes in response to the onset of polar conditions[25,26], the genomic substrate for reduced ossifications and buoyancy modifications had long been established, and was selected upon to facilitate the ecological diversification that characterizes the notothenioid adaptive radiation. These results provide an alternative view on the impact of climate change in driving extreme adaptations in the Southern Ocean[27,28]. As we march further into the Anthropocene, our results caution that as both ecosystems and climate continue to change worldwide, the expectation that rapid adaptation will be the dominant factor in predicting the response of biodiversity requires careful consideration[29].

Methods

Custom targeted sequence enrichment design. We based the design of the DNA enrichment baits primarily on the *N. coriiceps* genome, the species most closely related to those targeted for sequencing with a published reference assembly[30]. To account for regions that are unannotated, under drift, or not easily identified within the *N. coriiceps* assembly, we included targeted regions from several outgroup genomes as detailed below. By having the same element potentially represented by more than one genome, this strategy allowed us to mitigate against genome assembly and annotation artefacts while facilitating hybridization of diverse species to the capture probes. Elements were identified in the *N. coriiceps* genome using BLASTN (ncbi-blast-2.2.30+; parameters '*-max_target_seqs 1 -outfmt 6*'). If the BLASTN hit had an *E*-value < 0.0001 and covered >80% of the query sequence, we included this region from the *N. coriiceps* genome. If the region was not identified, or had <85% identity in *N. coriiceps*, we retained the version from the genome of origin.

Coding exons were identified from annotations of the *N. coriiceps*[30], stickleback (*Gasterosteus aculeatus*; BROADS1) and European sea bass (*Dicentrarchus labrax*) genomes[31]. CNEs were defined from the constrained elements identified in the stickleback and tilapia (*Oreochromis niloticus*; Orenil1.0) genomes from the Ensembl compara 11-way teleost whole-genome alignment[32]. We also included predicted miRNA hairpins from miRbase[33] and ultraconservative non-coding (UCNE) elements from UCNEbase[34]. miRNA hairpins were padded to be >100 bp. CNEs, miRNAs and UCNEs that overlapped coding exons were removed using Bedtools (v.2.26.0) intersectBed[35], and CNEs <100 bp were additionally excluded to facilitate space in the sequence capture design. Where the constrained regions that defined the CNEs overlapped with annotations pertaining to specific miRNAs and UCNEs, the latter annotations were prioritized.

Targeted elements were submitted to Nimblegen for final probe design, and the manufacturing of a Nimblegen SeqCap EZ Developer Library (Roche, No. 06471684001) had 63,838,670 bp of capture space targeting 318,929 elements from four reference genomes (88.9% *N. coriiceps*, 7.7% *G. aculeatus*, 3.0% *D. labrax*, 0.4% *O. nicoleatus*). Accounting for redundancy of orthologous target regions between the genomes, the final design targeted 258,176 unique elements of which 206,503 were predicted protein-coding exons and 51,673 constrained non-coding regions, with 85.0% coverage of targets not found in the *N. coriiceps* reference genome (47,097 elements; Supplementary Table 2).

Sample preparation and sequencing. Frozen tissue samples were acquired from the HWD and TJN laboratories, and from the Yale Peabody Museum frozen tissue collection (Supplementary Table 9). DNA from each species was isolated using Qiagen DNeasy Blood and Tissue kits, sequencing multiple individuals per species to account for population variation. For each species, equal amounts of DNA from each individual were pooled before shearing and library preparation. The pooled-population DNA was then sheared to an average size of 200 bp using the Covaris E220 ultrasonicator in 130 µl Covaris microTUBEs (duty cycle, 10%; intensity, 5; cycles/burst, 200; time, 300 s; temperature, 4 °C). Shearing was performed in shearing buffer: 10 mM Tris, 0.1 mM EDTA, pH 8.3.

Targeted sequence enrichment and next generation sequencing. Sequencing libraries were constructed from 1 µg of DNA using a KAPA Library Prep kit (Roche, No. 07137923001), following standard protocol with barcoding and dual-SPRI (solid phase reversible immobilisation) size selection to generate libraries of 200–450 bp. Sequencing libraries were hybridized, recovered and amplified according to the standard protocol (Nimblegen SeqCap EZ Library SR User's Guide v.4.3) with the following changes: hybridization was performed at 45 rather than 47 °C, to allow for more mismatches between sequencing libraries and probes, and we used SeqCap Developer Reagent (Roche, No. 06684335001) rather than Human CotI DNA to block non-specific hybridization as recommended by the protocol.

Since the majority of the capture probes were designed based on the sequence of *N. coriiceps*, we hybridized species in groups to limit potential competition between sequencing libraries of varied relatedness to the capture baits. Captured libraries were pooled for 100-bp, single-end sequencing using Illumina HiSeq 2500. We targeted multiplexing of eight to nine species per HiSeq 2500 flow cell, totalling six flow cells.

Reference contig assembly. The contig assembly approach is modified from the previously defined Phylomapping pipeline for cross-species targeted sequence enrichment datasets[15]. Briefly, sequencing reads are grouped into bins by homology to a targeted element (for example, exon, CNE) and then assembled into contigs de novo (Supplementary Fig. 7)

Processing of sequencing reads. Before contig assembly, low-quality bases within sequencing reads were masked using the FASTX-Toolkit (fastq_masker; parameters '-Q 33') (http://hannonlab.cshl.edu/fastx_toolkit). Illumina adaptor sequences were then trimmed using Trimmomatic v.0.36 (ref. [36]). Identical sequencing reads were collapsed using the FASTX-Toolkit v.0.0.13 (fastx_collapser; parameters '-Q 33').

Read binning into orthology groups by BLAST. Reads were grouped by homology before contig assembly, using both blastn and dc-megablast (v.2.6.0+, parameters '*-max_target_seqs 2 -outfmt 6*'). This dual-BLAST approach accounts for variation between sequencing reads and the reference genome from which the sequencing baits were defined[37]. As short target exons and CNEs can produce disproportionately small blastn *E* values, we used an adaptive *E* value cut-off based on the size of the target region. For target regions >25 bp, the cut-off was $E \leq 1 \times 10^{-5}$. For targets that were ≤25 bp the *E* value cut-off was $\leq 1 \times 10^{-4}$, and for targets that were ≤20 bp the *E* value cut-off was $\leq 1 \times 10^{-3}$. Reads were further excluded if a substantial portion of the read (>10 bp) overlapped the target interval without being included in a blastn hit. The best resulting *E* value from either blastn or dc-megablast was selected, with the former selected in the event of a tie. As dc-megablast uses a mismatch-tolerant seed template, inclusion of dc-megablast resulted in the additional recovery of 30,000–50,000 sequencing reads per species (out of an average of 20,000,000 with total blastn hits) and the assembly of 50–150 more target regions than would be assembled by blastn alone.

De novo contig assembly. CAP3 was used to assemble contigs de novo from the bins of reads that have high homology to specific target regions (that is, the same exon, CNE and so on) that were identified by BLAST[38]. Reads were reverse-complemented if necessary to put everything into the same complement strand as the target region from the reference genome. To accelerate CAP3 assembly, overlapping reads were first merged into smaller contigs using Usearch and then mixed with original reads as input for CAP3 (parameters '-id 0.97 -fastq_maxdiffs 3 -fastq_minovlen 5'). For CAP3 assembly, we required a minimum read overlap of 16 bp and 96% identity between reads during contig assembly (parameters '-o 16 -p 96'). This cut-off has an effect of separating the reads stemming from duplication events into separate contigs, providing there is >4–6% variance between the paralogous regions.

We simulated the ability of this pipeline to distinguish copy number variants (Supplementary Fig. 8a), generating a 300-bp random DNA sequence in silico and making a second copy of this sequence with specific levels of variation from the original. Sequencing reads (100 bp) were then generated in silico at a depth of one read every five base pairs. Reads were run through the assembly pipeline to assess whether the original DNA sequences were reconstructed from the read data,

or whether the reads formed a chimeric sequence. This simulation was repeated 250 times. The current assembly approach was able to reassemble the individual paralogues where there was >6% divergence between original paralogous sequences, with inconsistent results at <5% divergence (Supplementary Fig. 8b).

Contig merging and filtering. Sequencing reads were aligned to the assembled contigs using NextGenMap (v.0.5.5; parameters '-R 40')[39]. This alignment step allows for the recruitment of new reads to the contig that may not have previously been identified by blastn due to either high degrees of variance relative to the reference blast database, large indels or low amounts of overlapping sequence with the target region. This allows elongation of the contig to include more of the flanking regions surrounding each target element. Reads were removed from the alignment to the contig if there were more than three mismatches with the exception of indels. To refine and extend the boundaries of the original contig, a second de novo assembly by CAP3 (parameters '-o 20 -p 85') was performed using the aligned reads.

Multiple contigs were present in around 65% of target regions after CAP3 assembly. To remove misidentified contigs, we used blastn to compare each contig to the reference genome, removing those whose top hit did not match the original bin from which the reads were assembled. To correct for potential assembly artefacts, the multiple contigs that represent each target were compared to each other and the reference sequence in a multiple sequence alignment using Mafft v.7.313 (ref. [40]) (parameters '–maxiterate 1000 –localpair'), adding contigs as fragments (parameters '–addfragments'). Using the read support at each base in the alignment, we generated a consensus contig sequence for each target region. A mismatch between contigs was considered if the read support for the most common base was <80% of all bases present. Contigs were merged only if there were less than 3 mismatches, if the sequence identity between the contigs was >95% or if the contigs did not overlap within the target region. After this refinement step, <2% of target regions were represented by multiple contigs.

Comparison of assembled contigs to reference genome. In comparing our reference exome sequence assembly to the published *N. coriiceps* reference genome, we found 99.8% average percentage identity of exome sequence to the reference target (Supplementary Fig. 9), which included 98.5% of exons in the *N. coriiceps* reference genome (Supplementary Fig. 9). The small differences in sequence identity and putative copy-number variants (CNVs) between this exome and the genome assembly may reflect meaningful biological variation in our independently sampled *N. coriiceps* populations. Both the sequence composition of the assembled exome and the predicted copy number data closely match the whole-genome sequence data, providing confidence in our assembly.

Estimation of read coverage and depth of targeted regions. Coverage was estimated using BEDtools (v.2.23.0)[35]. Reads were first aligned to the assembled contigs with NextGenMap[39]. The coordinates of the read alignments were then lifted to the corresponding position on the reference genome using information from a pairwise sequence alignment between the contig and the orthologous region on the reference genome. Pairwise alignments were performed using Biopython v.1.70 (parameters 'pairwise2; match = 5, mismatch = −4, gap_open = −15, gap_extend = −1'). Alignments were converted to BAM files, sorted and indexed using SAMtools v.1.9 (ref. [41]). Reads alignments were manually inspected in the Integrative Genome Viewer to verify accurate read alignment[42]. Coverage is defined as the percentage of targeted bases in the primary reference genome having at least one read. Depth was estimated using coverageBed (parameters '-d').

Distribution of read coverage across the dataset. Most target regions had either 0 or 100% coverage (Supplementary Fig. 10). Although the average depth is similar in the notothenioids compared to the outgroups, there is a wider distribution of depths in outgroup species (Supplementary Fig. 10). Despite global coverage being ≥85% in all species, gene classes associated with the immune system, cell adhesion proteins and extracellular matrix were enriched among regions with relatively poor coverage (<25% coverage in ≥75% of exons; Supplementary Table 10). This suggests that these fast-evolving gene classes are less likely to be highly represented in these datasets, and is similar to previous findings with cross-species-targeted DNA enrichment[43].

Recovery of population variation. To determine the ability of this approach to recover population variation, we looked for heterozygous SNPs within the targeted regions of the dataset. Sequencing reads were aligned to the reference contigs for each species using NextGenMap[39]. SAM files were converted to BAM files using SAMtools v.1.9 (ref. [41]). Variants were called using SAMtools mpileup and BCFtools v.1.9 (parameters 'call -mv'). We considered sites heterozygous in our small population samples if there were at least two reads showing the variant in at least 25% allele frequency within the sequencing reads.

Treatment of exons with a predicted history of duplication. We assembled a single exon/CNE copy for the majority of targets that were directly compared between species. However, less than 3% of targeted regions on average had assembled more than one contig per target region after assembly. For duplicated regions, both exon versions were ignored for that particular species in downstream analyses involving multiple groups, unless those analyses ask specific questions involving copy number.

Identification of orthologous sequences. For orthologue pairing, the contigs generated from the same reference target region were aligned using Mafft v.7.313 (parameters '–op 10–ep 10')[40], with a maximum likelihood tree topology estimated IQTree[44]. Gene trees were reconciled with the species tree using Notung-2.9 (ref. [45]) (parameters '–reconcile–rearrange–silent–threshold 90%–treeoutput nhx') to infer patterns of duplication and loss. The total number of duplication and loss events inferred by Notung was then summed and compared to a null scenario where all copies are local duplicates. If Notung inferred fewer gain/loss events, the duplicate exons were paired based on the reconciled gene tree.

Simulation of orthologue identification approach. To estimate the ability of this approach to parse copy number variation into orthologous groups, we performed a series of simulations (Supplementary Fig. 11a) using a random DNA sequence generated in silico. This ancestral DNA sequence was duplicated, and mutations were added at defined levels to distinguish each paralogue. Both paralogues were then evolved according to a specified phylogeny, with variation added to each paralogue in increments at each branch point. We varied copy number, length of contig sequence and simulated local losses of an individual paralogue within downstream lineages. Each simulation was repeated 250 times. These results suggest that, providing there is ≥4–6% variation between paralogous sequences, the approach can properly pair orthologous sequences (Supplementary Fig. 11b–d). This coincides with the thresholds at which our pipeline can distinguish copy number variants during contig assembly (see above), meaning that there will not be paralogue sequences with <4% divergence in the dataset.

Multiple sequence alignment. All paired orthologous sequences were aligned using Mafft v.7.313 (parameters '–maxiterate 1000 –localpair –op 10 –ep 10'). For coding regions that had out-of-frame or frameshift-causing indels, these alignments were then refined into codon alignments using the frameshift-aware multiple sequence aligner MACSE v.2.03 (parameters '-prog alignSequences -seq -seq_lr -fs_lr 10 -stop_lr 15')[46]. The multiple sequence alignment was pruned using GUIDANCE v.2.02 to mask residues with score <0.6 (parameters '–bootstrap 25 –mafft–maxiterate 100 –localpair –op 10 –ep 10')[47].

Reconstruction of gene sequences from exon data. Single-copy coding exons with orthology to *G. aculeatus* were concatenated into gene sequences using the annotations of the *G. aculeatus* genome. The exons for each gene were spliced together in the same order in which they appear in the genome on the strand containing the gene. Transcript isoforms were merged into a non-redundant gene sequence containing all possible exons. A total of 18,600 gene sequences with orthology to *G. aculeatus* were reconstructed for each species.

Notothenioid phylogeny. We used two approaches to infer a phylogeny for notothenioids. For both analyses, only single-copy genes with >85% coverage in all species were included, resulting in a dataset of 11,627 genes. First, we individually partitioned each gene by codon position and used ModelFinder as implemented in IQTree v.1.6.3 (ref. [48]) to estimate the optimal partitioning scheme and molecular evolution model. The gene set was concatenated into a single sequence, and a maximum likelihood tree was inferred using IQTree v.1.6.3 (ref. [44]). To assess support for the phylogenetic relationships, we performed 1,000 ultra-fast bootstrap replicates[49].

To account for the effects of incomplete lineage sorting and known issues with concatenation for phylogenetic inference[50,51], we also inferred a species tree. Full species tree inference is not computationally feasible with large genomic datasets, so we relied on the summary species tree approach in ASTRAL v.5.6.2 (ref. [52]). We first used IQTree v.1.6.3 to infer the maximum likelihood tree for each gene, applying partitioning schemes and molecular evolution models as described above. We then used ASTRAL to summarize the distribution of gene trees and estimate the species tree. To assess support for the species tree topology, we estimated local posterior probabilities for each quadpartition in the tree[53].

Quantification of lineage diversification dynamics. To test for changes in lineage diversification rates across the temporal history notothenioids, we used a Bayesian analysis of macro-evolutionary mixtures implemented in BAMM v.2.5 with a previously published time-tree that sampled all major lineages and 87 of ~120 species of notothenioids[11]. Priors were were defined using the function setBAMMpriors contained in the R package BAMMtools v.2.1.0 (ref. [54]) and missing species were accounted for based on currently described species, with outgroup sampling capturing all major lineages of non-polar notothenioids. BAMM was run for 100 million generations and assessed for target sampling of the posterior distribution (effective sample size >200). Results were visualized using functions available from the R package BAMMtools[54]. To assess the impact of phylogenetic uncertainty in topology and branch lengths on our estimates of speciation rates through time, we further replicated the above analysis across 500 topologies randomly selected from the posterior distribution of trees from the same previous work[11] (Supplemental Fig. 12).

dS and dN estimates of substitution rate. The criteria dN, dS and dN/dS were calculated pairwise between each species and the outgroup *Percina caprodes*. This was performed for each reconstructed gene of at least 2,000 bp in both species using cal_dn_ds in the Biopython v.1.70 codonseq module (parameters 'method = "NG86" '). The values of dN, dS and dN/dS were then averaged across all genes for each species.

Molecular clock models of substitution rate. Substitution rates were estimated from the reconstructed gene sequences using the random local clock model as implemented in BEAST v.2.4.8 (codon partitioned, bModelTest, parameters 'chain length = 30M')[55–57]. To simplify comparisons between gene trees, and because support for the relationships between the included species is high, we fixed the starting tree topology for each gene tree to match our ASTRAL-inferred species tree (Supplementary Fig. 13). Only gene trees with an effective sample size (ESS) ≥ 200 for all parameters were selected for downstream analysis (total 1,062). Most recent common ancestor (MRCA) age priors were calibrated based on previous age estimates[11,58]: *Psuedaphritis* + Eleginopsioidea 63.0 Ma (52.6–73.4), Bovichtidae + all notothenioids 85.7 Ma) (69.5–102.6), *Harpagifer-Pogonophryne* 10.2 Ma (7.7–13.0), *Bathydraco-Chaenocephalus* 11.1 Ma (9.4–13.3), *Notothenia* 17.7 Ma (15.2–20.5), Cryonotothenioidea 21.6 Ma (18.6–23.9), Eleginopsioidea 45.9 Ma (37.2–53.2). The maximum clade credibility was constructed for each gene tree using TreeAnnotator.

Detection of diversifying selection. Positive selection was calculated using the adaptive branch-site random effects likelihood (aBSREL) implemented in HyPhy v.2.3.9 (refs. [59,60]). Single-copy exon alignments were concatenated into genes as input based on the gene order in the stickleback genome. The species tree was used for all comparisons (Supplementary Fig. 13). Accelerated sequence evolution was assessed using phyloP[61] as implemented in PHAST v.1.4 (ref. [62]) (parameters '–method LRT–no-prune–features–mode ACC'). The tree model for phyloP was derived separately for CNE and coding gene comparisons using phyloFit and the species tree (Supplementary Fig. 13). Tree models for protein-coding regions were based on 3,381 exons ≥1,000 bp with ≥85% coverage in all species. CNE tree models were based on 2,912 elements ≥250 bp with ≥85% coverage in all species.

Ontology enrichment. As there are no gene ontology terms relating to *N. coriiceps*, we generated a custom gene ontology database based on the combined gene ontology data from multiple species. Gene ontology data were mined from chicken, mouse, rat, human, stickleback, medaka and zebrafish in Ensembl BioMart (downloaded December 2016)[63]. All Ensembl gene IDs were converted to their Ensembl stickleback orthologue and a final merged gene ontology list was created by combining stickleback orthologues for each species. Because many of the evolved phenotypes in notothenioids are comparable to human pathologies, we further used human phenotype ontology (HPO) databases to characterize genetic trends within the fish dataset[64]. This database (downloaded April 2018) was then converted from human to stickleback orthologues using Ensembl BioMart.

Ontology enrichment was performed using Fisher's exact test (SciPy v.0.18.1; fisher_exact). We also assessed patterns of cumulative polygenic enrichment within ontologies using the SUMSTAT approach as implemented in ref. [65]. This approach normalizes the distribution of log-likelihood ratio test values (ΔlnL) output from phyloP and HyPhy by taking the fourth root (ΔlnL4). The ΔlnL4 score is then summed for all genes within an ontology, and an enrichment *P* value is estimated from the empirical sum(ΔlnL4) score through bootstrap resampling (1,500 replicates). For all enrichment analyses, *P* values were corrected using false discovery rate (python module statsmodels v.0.6.1; fdrcorrection0).

Zebrafish husbandry and genetic lines. Zebrafish WT and mutant lines used were housed and maintained as previously described and in accordance with Boston Children's Hospital IACUC regulations[66]. The *col1a1a* (dmh14) and *col1a2* (dmh15) mutants were derived from a forward genetic screen[43].

Zebrafish genome editing. The guide RNA (gRNA) site GGTCAGAGTTTGGGTCAGGTCGG in exon 1 of the zebrafish *trip11* gene was targeted. This site is 33 bp downstream of the ATG start codon of *trip11*. gRNA sequences were cloned in the BsaI site of the DR274 plasmid and in vitro transcribed with the T7 RNAmax kit (ThermoFisher). Cas9 messenger RNA was obtained from SystemBio (CAS500A-1). Injections of fertilized zebrafish eggs were done with 50 ng ul^{-1} gRNA and 150 ng ul^{-1} Cas9 mRNA. Genotyping was performed using 5′-CCCTGGTCGGTGATTTAGGGTTAG-3′ as forward primer and 5′ CA CCTCCCACTTCCTCGGCGCTTTCCAGCAGAATATCTTTGGTAAAATTAG AG-3′ as reverse primer. PCRs using this primer pair yield a 178-bp WT band. Fish were identified with a 47-bp deletion spanning the gRNA target site and yielding a 131-bp genotyping band. The deleted sequence is 5′-CTGGGTCAGAGTTTGGG TCAGGTCGGGGGAAGCTTGTCTTCATTTAC-3′ and generates a frameshift at the 12th amino acid residue of *trip11*.

Analysis of skeletal density through computed tomography. Adult notothenioid specimens were loaned from the Yale Peabody Museum and Harvard Museum of Comparative Zoology (Supplementary Table 11) and scanned using the Siemens Biograph at Boston Children's Hospital Department of Nuclear Medicine and Molecular Imaging. Scan data were processed in Siemens PETsyngo VG60A software and analysed in Amira (v.6.0.0, FEI Inc.).

Zebrafish were euthanized in 22% MS-222, fixed in 3.7% formaldehyde overnight and rinsed in phosphate buffered saline. The fishes were embedded in 1% agarose to reduce movement during imaging. The fish skulls were scanned as in ref. [19] using a Skyscan 1173 (Bruker), 240-degree scan with 0.2 rotational step; X-ray source voltage set to 70 kV and current set to 80 µA; exposure time was 1,500 ms and resolution of scans was 7.14 microns per pixel. Volume renderings were reconstructed as maximum intensity projections in Amira software. Skeletal density was estimated based on the average pixel intensity measured from the maximum intensity projection of the skull, vertebrae and operculum in ImageJ v.1.51 s (https://imagej.nih.gov/ij/). A total of $n = 6$ *trip11*$^{+/-}$ and $n = 10$ *trip11*$^{-/-}$ fish were scanned and quantified. The bones of the skull roof (parietal/frontal), operculum and vertebrae were measured from each individual.

Reporting Summary. Further information on research design is available in the Nature Research Reporting Summary linked to this article.

Data availability

The sequencing data have been deposited in the NCBI database as Bioproject PRJNA531677. Assembled contig data have been deposited in the Zenodo repository (10.5281/zenodo.2628936).

Received: 27 December 2018; Accepted: 2 May 2019;
Published online: 10 June 2019

References

1. Schluter, D. *The Ecology of Adaptive Radiation* (Oxford Univ. Press, 2000).
2. Chan, Y. F. et al. Adaptive evolution of pelvic reduction of a Pitx1 enhancer. *Science* **327**, 302–306 (2010).
3. Santos, M. E. et al. The evolution of cichlid fish egg-spots is linked with a cis-regulatory change. *Nat. Commun.* **5**, 5149 (2014).
4. Rabosky, D. L. Phylogenetic tests for evolutionary innovation: the problematic link between key innovations and exceptional diversification. *Phil. Trans. R. Soc. B* **372**, 20160417 (2017).
5. Stroud, J. T. & Losos, J. B. Ecological opportunity and adaptive radiation. *Annu. Rev. Ecol. Evol. Syst.* **47**, 507–532 (2016).
6. Losos, J. B. *Lizards in an Evolutionary Tree: Ecology and Adaptive Radiation of Anoles* (Univ. of California Press, 2009).
7. Gould, S. J. *Wonderful Life: The Burgess Shale and the Nature of History* (W. W. Norton & Co., 1989).
8. Gould, S. J. *The Structure of Evolutionary Theory* (Harvard Univ. Press, 2002).
9. Jablonski, D. Approaches to macroevolution: 1. General concepts and origin of variation. *Evol. Biol.* **44**, 427–450 (2017).
10. Near, T. J. et al. Ancient climate change, antifreeze, and the evolutionary diversification of Antarctic fishes. *Proc. Natl Acad. Sci. USA* **109**, 3434–3439 (2012).
11. Dornburg, A., Federman, S., Lamb, A. D., Jones, C. D. & Near, T. J. Cradles and museums of Antarctic teleost biodiversity. *Nat. Ecol. Evol.* **1**, 1379–1384 (2017).
12. Eastman, J. T. *Antarctic Fish Biology: Evolution in a Unique Environment* (Academic Press, Inc., 1993).
13. DeVries, A. L. & Eastman, J. T. Lipid sacs as a buoyancy adaptation in an Antarctic fish. *Nature* **271**, 352–353 (1978).
14. Eastman, J. T., Witmer, L. M., Ridgely, R. C. & Kuhn, K. L. Divergence in skeletal mass and bone morphology in Antarctic notothenioid fishes. *J. Morphol.* **275**, 841–861 (2014).
15. Daane, J. M., Rohner, N., Konstantinidis, P., Djuranovic, S. & Harris, M. P. Parallelism and epistasis in skeletal evolution identified through use of phylogenomic mapping strategies. *Mol. Biol. Evol.* **33**, 162–173 (2016).
16. Near, T. J., Parker, S. K. & Detrich, H. W. A genomic fossil reveals key steps in hemoglobin loss by the Antarctic icefishes. *Mol. Biol. Evol.* **23**, 2008–2016 (2006).
17. Brawand, D. et al. The genomic substrate for adaptive radiation in African cichlid fish. *Nature* **513**, 375–381 (2014).
18. Rabosky, D. L. Automatic detection of key innovations, rate shifts, and diversity-dependence on phylogenetic trees. *PLoS ONE* **9**, e89543 (2014).
19. Gistelinck, C. et al. Zebrafish type I collagen mutants faithfully recapitulate human type I collagenopathies. *Proc. Natl Acad. Sci. USA* **115**, E8037–E8046 (2018).
20. Van Dijk, F. S. & Sillence, D. O. Osteogenesis imperfecta: clinical diagnosis, nomenclature and severity assessment. *Am. J. Med. Genet. A* **164**, 1470–1481 (2014).
21. Albertson, R. C. et al. Molecular pedomorphism underlies craniofacial skeletal evolution in Antarctic notothenioid fishes. *BMC Evol. Biol.* **10**, 4 (2010).

22. Witkos, T. M. & Lowe, M. The golgin family of coiled-coil tethering proteins. *Front. Cell Dev. Biol.* **3**, 86 (2016).
23. Smits, P. et al. Lethal skeletal dysplasia in mice and humans lacking the golgin GMAP-210. *N. Engl. J. Med.* **362**, 206–216 (2010).
24. Eastman, J. T. & McCune, A. R. Fishes on the Antarctic continental shelf: evolution of a marine species flock? *J. Fish Biol.* **57**, 84–102 (2000).
25. Chen, L., DeVries, A. & Cheng, C. Evolution of antifreeze glycoprotein gene from a trypsinogen gene in Antarctic notothenioid fish. *Proc. Natl Acad. Sci. USA* **94**, 3811–3816 (1997).
26. Chen, Z. et al. Transcriptomic and genomic evolution under constant cold in Antarctic notothenioid fish. *Proc. Natl Acad. Sci. USA* **105**, 12944–12949 (2008).
27. Chown, S. L. et al. The changing form of Antarctic biodiversity. *Nature* **522**, 431–438 (2015).
28. Chown, S. L. et al. Antarctica and the strategic plan for biodiversity. *PLoS Biol.* **15**, e2001656 (2017).
29. Bilyk, K. T., Vargas-Chacoff, L. & Cheng, C. H. C. Evolution in chronic cold: varied loss of cellular response to heat in Antarctic notothenioid fish. *BMC Evol. Biol.* **18**, 143 (2018).
30. Shin, S. C. et al. The g enome sequence of the Antarctic bullhead notothen reveals evolutionary adaptations to a cold environment. *Genome Biol.* **15**, 468 (2014).
31. Tine, M. et al. European sea bass genome and its variation provide insights into adaptation to euryhalinity and speciation. *Nat. Commun.* **5**, 5770 (2014).
32. Herrero, J. et al. Ensembl comparative genomics resources. *Database* **2016**, bav096 (2016).
33. Kozomara, A. & Griffiths-Jones, S. MiRBase: integrating microRNA annotation and deep-sequencing data. *Nucleic Acids Res.* **39**, D152–D157 (2011).
34. Dimitrieva, S. & Bucher, P. UCNEbase - a database of ultraconserved non-coding elements and genomic regulatory blocks. *Nucleic Acids Res.* **41**, 101–109 (2013).
35. Quinlan, A. R. & Hall, I. M. BEDTools: a flexible suite of utilities for comparing genomic features. *Bioinformatics* **26**, 841–842 (2010).
36. Bolger, A. M., Lohse, M. & Usadel, B. Trimmomatic: a flexible trimmer for Illumina sequence data. *Bioinformatics* **30**, 2114–2120 (2014).
37. Altschul, S., Gish, W. & Miller, W. Basic local alignment search tool. *J. Mol. Biol.* **215**, 403–410 (1990).
38. Huang, X. CAP3: a DNA sequence assembly program. *Genome Res.* **9**, 868–877 (1999).
39. Sedlazeck, F. J., Rescheneder, P. & Von Haeseler, A. NextGenMap: fast and accurate read mapping in highly polymorphic genomes. *Bioinformatics* **29**, 2790–2791 (2013).
40. Katoh, K., Kuma, K., Toh, H. & Miyata, T. MAFFT version 5: improvement in accuracy of multiple sequence alignment. *Nucleic Acids Res.* **33**, 511–518 (2005).
41. Li, H. et al. The sequence alignment/map format and SAMtools. *Bioinformatics* **25**, 2078–2079 (2009).
42. Robinson, J. T. et al. Integrative genome viewer. *Nat. Biotechnol.* **29**, 24–26 (2011).
43. Henke, K. et al. Genetic screen for post-embryonic development in the zebrafish (*Danio rerio*): dominant mutations affecting adult form. *Genetics* **207**, 609–623 (2017).
44. Nguyen, L. T., Schmidt, H. A., Von Haeseler, A. & Minh, B. Q. IQ-TREE: a fast and effective stochastic algorithm for estimating maximum-likelihood phylogenies. *Mol. Biol. Evol.* **32**, 268–274 (2015).
45. Chen, K., Durand, D. & Farach-Colton, M. NOTUNG: a program for dating gene duplications and optimizing gene family trees. *J. Comput. Biol.* **7**, 429–447 (2000).
46. Ranwez, V., Harispe, S., Delsuc, F. & Douzery, E. J. P. MACSE: multiple alignment of coding SEquences accounting for frameshifts and stop codons. *PLoS ONE* **6**, e22594 (2011).
47. Sela, I., Ashkenazy, H., Katoh, K. & Pupko, T. GUIDANCE2: accurate detection of unreliable alignment regions accounting for the uncertainty of multiple parameters. *Nucleic Acids Res.* **43**, W7–W14 (2015).
48. Kalyaanamoorthy, S., Minh, B. Q., Wong, T. K. F., Von Haeseler, A. & Jermiin, L. S. ModelFinder: fast model selection for accurate phylogenetic estimates. *Nat. Methods* **14**, 587–589 (2017).
49. Hoang, D. T., Chernomor, O., Von Haeseler, A., Minh, B. Q. & Vinh, L. S. UFBoot2: improving the ultrafast bootstrap approximation. *Mol. Biol. Evol.* **35**, 518–522 (2018).
50. Kubatko, L. S. & Degnan, J. H. Inconsistency of phylogenetic estimates from concatenated data under coalescence. *Syst. Biol.* **56**, 17–24 (2007).
51. Roch, S. & Steel, M. Likelihood-based tree reconstruction on a concatenation of aligned sequence data sets can be statistically inconsistent. *Theor. Popul. Biol.* **100**, 56–62 (2015).
52. Zhang, C., Rabiee, M., Sayyari, E. & Mirarab, S. ASTRAL-III: polynomial time species tree reconstruction from partially resolved gene trees. *BMC Bioinformatics* **19**, 15–30 (2018).
53. Sayyari, E. & Mirarab, S. Fast coalescent-based computation of local branch support from quartet frequencies. *Mol. Biol. Evol.* **33**, 1654–1668 (2016).
54. Rabosky, D. L. et al. BAMMtools: an R package for the analysis of evolutionary dynamics on phylogenetic trees. *Methods Ecol. Evol.* **5**, 701–707 (2014).
55. Bouckaert, R. et al. BEAST 2: a software platform for Bayesian evolutionary analysis. *PLoS Comput. Biol.* **10**, e1003537 (2014).
56. Bouckaert, R. R. & Drummond, A. J. bModelTest: Bayesian phylogenetic site model averaging and model comparison. *BMC Evol. Biol.* **17**, 42 (2017).
57. Drummond, A. J. & Suchard, M. A. Bayesian random local clocks, or one rate to rule them all. *BMC Biol.* **8**, 114 (2010).
58. Near, T. J. et al. Identification of the notothenioid sister lineage illuminates the biogeographic history of an Antarctic adaptive radiation. *BMC Evol. Biol.* **15**, 109 (2015).
59. Smith, M. D. et al. Less is more: an adaptive branch-site random effects model for efficient detection of episodic diversifying selection. *Mol. Biol. Evol.* **32**, 1342–1353 (2015).
60. Kosakovsky Pond, S. L., Frost, S. D. W. & Muse, S. V. HyPhy: hypothesis testing using phylogenies. *Bioinformatics* **21**, 676–679 (2005).
61. Pollard, K. S., Hubisz, M. J., Rosenbloom, K. R. & Siepel, A. Detection of nonneutral substitution rates on mammalian phylogenies. *Genome Res.* **20**, 110–121 (2010).
62. Hubisz, M. J., Pollard, K. S. & Siepel, A. PHAST and RPHAST: phylogenetic analysis with space/time models. *Brief. Bioinforma.* **12**, 41–51 (2011).
63. Kinsella, R. J. et al. Ensembl BioMarts: a hub for data retrieval across taxonomic space. *Database* **2011**, bar030 (2011).
64. Köhler, S. et al. The human phenotype ontology in 2017. *Nucleic Acids Res.* **45**, D865–D876 (2017).
65. Daub, J. T., Moretti, S., Davydov, I. I. & Excoffier, L. Detection of pathways affected by positive selection in primate lineages ancestral to humans. *Mol. Biol. Evol.* **34**, 1391–1402 (2017).
66. Nüsslein-Volhard, C. & Dahm, R. *Zebrafish: A Practical Approach* (Oxford Univ. Press, 2002).

Acknowledgements

The authors thank E. Snay and L. Oberg in the Department of Nuclear Medicine and Molecular Imaging at Boston Children's Hosptial for assistance in computed tomography of adult specimens. This work was supported in part by American Heart Association Postdoctoral Fellowship (No. 17POST33660801) to J.M.D., the John Simon Guggenheim Fellowship and William F. Milton Fund awarded to M.P.H., the National Science Foundation (NSF) grant (No. PLR-1444167 to H.W.D.), the NSF grant (No. IOS-1755242 to A.D.), the Bingham Oceanographic Fund from the Peabody Museum of Natural History, and Yale University, as well as the Children's Orthopaedic Surgery Foundation at Boston Children's Hospital. This is contribution No. 389 from the Marine Science Center at Northeastern University.

Author contributions

J.M.D., H.W.D. and M.P.H. conceived and designed the study. J.M.D., P.S. and M.B.H. performed the experiments. J.M.D., A.D., T.J.N., D.J.M., H.W.D. and M.P.H. analysed the data. J.M.D., A.D. and T.J.N. wrote the first drafts of the manuscript. All authors contributed to the writing of the final manuscript.

Competing interests

The authors declare no competing interests.

Additional information

Supplementary information is available for this paper at https://doi.org/10.1038/s41559-019-0914-2.

Reprints and permissions information is available at www.nature.com/reprints.

Correspondence and requests for materials should be addressed to J.M.D., H.W.D. or M.P.H.

Publisher's note: Springer Nature remains neutral with regard to jurisdictional claims in published maps and institutional affiliations.

nature research

Corresponding author(s): Jacob M. Daane
H.William Detrich II
Matthew P. Harris

Last updated by author(s): 5-1-19

Reporting Summary

Nature Research wishes to improve the reproducibility of the work that we publish. This form provides structure for consistency and transparency in reporting. For further information on Nature Research policies, see Authors & Referees and the Editorial Policy Checklist.

Statistics

For all statistical analyses, confirm that the following items are present in the figure legend, table legend, main text, or Methods section.

n/a	Confirmed	
☐	☒	The exact sample size (*n*) for each experimental group/condition, given as a discrete number and unit of measurement
☐	☒	A statement on whether measurements were taken from distinct samples or whether the same sample was measured repeatedly
☐	☒	The statistical test(s) used AND whether they are one- or two-sided *Only common tests should be described solely by name; describe more complex techniques in the Methods section.*
☒	☐	A description of all covariates tested
☐	☒	A description of any assumptions or corrections, such as tests of normality and adjustment for multiple comparisons
☐	☒	A full description of the statistical parameters including central tendency (e.g. means) or other basic estimates (e.g. regression coefficient) AND variation (e.g. standard deviation) or associated estimates of uncertainty (e.g. confidence intervals)
☐	☒	For null hypothesis testing, the test statistic (e.g. *F*, *t*, *r*) with confidence intervals, effect sizes, degrees of freedom and *P* value noted *Give P values as exact values whenever suitable.*
☐	☒	For Bayesian analysis, information on the choice of priors and Markov chain Monte Carlo settings
☒	☐	For hierarchical and complex designs, identification of the appropriate level for tests and full reporting of outcomes
☒	☐	Estimates of effect sizes (e.g. Cohen's *d*, Pearson's *r*), indicating how they were calculated

Our web collection on statistics for biologists contains articles on many of the points above.

Software and code

Policy information about availability of computer code

Data collection	Skeletal computed tomography (CT) scans of notothenioids were processed in Siemens PETsyngo VG60A. No other software was used in the collection of the data
Data analysis	The following programs were used in the processing and analysis of the data: BAMMtools (v2.1.0) -- lineage diversification rate analysis BEAST (v2.4.8) -- substitution rate analysis HYPHY (v2.3.9) -- positive selection through aBSREL program PHAST (v1.4) -- accelerated sequence evolution through phyloP program Python SciPy (v0.18.1) -- Fisher's exact test for GO-enrichment (fisher_exact) Python statsmodels (v0.6.1) -- multiple hypothesis test correction (fdrcorrection0) IQTree (v.1.6.3) -- gene trees ASTRAL (v.5.6.2) --species tree from gene trees Sequencing read processing and contig assembly programs: Trimmomatic (v0.3) FASTX-Toolkit (v0.0.13) blastn (ncbi-blast-2.2.30+) dc-megablast (v2.6.0+) Biopython (v1.70) -- codonseq and pairwise2 modules BEDtools (v2.23.0) CAP3 (02/10/15) Notung (v2.9) Multiple sequence alignment and alignment pruning : MACSE (v2.03)

Mafft (v7.313)
GUIDANCE (v2.02)

Read alignment:
NextGenMap (v0.5.5)
SAMtools (v1.9)
BCFtools (v1.9)

Processing and analysis of CT scans:
ImageJ (v1.51s)
Amira (v6.0.0)
Siemens PETsyngo VG60A

For manuscripts utilizing custom algorithms or software that are central to the research but not yet described in published literature, software must be made available to editors/reviewers. We strongly encourage code deposition in a community repository (e.g. GitHub). See the Nature Research guidelines for submitting code & software for further information.

Data

Policy information about availability of data

All manuscripts must include a data availability statement. This statement should provide the following information, where applicable:

- Accession codes, unique identifiers, or web links for publicly available datasets
- A list of figures that have associated raw data
- A description of any restrictions on data availability

The sequencing reads have been deposited on the NCBI SRA (Bioproject PRJNA531677). Assembled contigs and annotations for all species in the dataset have been uploaded to the Zenodo repository (doi: 10.5281/zenodo.2628936).

Field-specific reporting

Please select the one below that is the best fit for your research. If you are not sure, read the appropriate sections before making your selection.

☒ Life sciences ☐ Behavioural & social sciences ☐ Ecological, evolutionary & environmental sciences

For a reference copy of the document with all sections, see nature.com/documents/nr-reporting-summary-flat.pdf

Life sciences study design

All studies must disclose on these points even when the disclosure is negative.

Sample size	We started with a goal of n>5 and >10 for control and experimental groups respectively for analysis of trip11 zebrafish mutants, with these numbers selected to capture variation in the phenotype while minimizing the usage of laboratory animals.
Data exclusions	No data were excluded from the analysis
Replication	Zebrafish trip11 mutant individuals were scanned from two independent genetic crosses.
Randomization	As the zebrafish work focused on defined genotypes, we did not randomize into experimental groups for zebrafish experiments. Further, no randomization was necessary in the genomic analysis, as this analysis is predicated on questions at specific places within the phylogeny
Blinding	Investigators were not blinded to the genotypic and genomic data analysis. As the research questions focused on specific lineages within the phylogeny, blinding would not be possible.

Reporting for specific materials, systems and methods

We require information from authors about some types of materials, experimental systems and methods used in many studies. Here, indicate whether each material, system or method listed is relevant to your study. If you are not sure if a list item applies to your research, read the appropriate section before selecting a response.

Materials & experimental systems

n/a	Involved in the study
☒	☐ Antibodies
☒	☐ Eukaryotic cell lines
☒	☐ Palaeontology
☐	☒ Animals and other organisms
☒	☐ Human research participants
☒	☐ Clinical data

Methods

n/a	Involved in the study
☒	☐ ChIP-seq
☒	☐ Flow cytometry
☒	☐ MRI-based neuroimaging

Animals and other organisms

Policy information about studies involving animals; ARRIVE guidelines recommended for reporting animal research

Laboratory animals	This study involves the use of zebrafish (Danio rerio). Both genders between the ages of 3-6 months were used. Mutant strains include col1a1a (dmh14) and col1a2 (dmh15). CRISPR mutants in trip11 were generated from wild-type strains.
Wild animals	This study did not involve wild animals
Field-collected samples	No tissue samples were directly collected from the field for the purposes of this study. Tissue samples were obtained from the Yale Peabody frozen tissue collection and from the laboratory collection of H.W. Detrich from previously published Antarctic expeditions. Adult notothenioid specimens were also loaned from the Yale Peabody Museum for CT scanning. Full sample and specimen identifiers are available in the Supplement.
Ethics oversight	Boston Children's Hospital Institutional Animal Care and Use Committee (IACUC).

Note that full information on the approval of the study protocol must also be provided in the manuscript.